MHD Simulations of Parker Instability Undergoing Cosmic-Ray Diffusion: Effect of the Initial Equilibrium Conditions on Mixing

Ying-Yi Lo, Chih-Yueh Wang[1,]

Department of Physics, Chung-Yuan Christian University, 200 Chung-Pei Road, Chung-Li, Taiwan 32023

Abstract

Parker instability arises from the presence of magnetic fields in a plasma such as the interstellar medium (ISM), wherein the magnetic buoyant pressure expels the gas and causes the gas to move along the field lines. The subsequent gravitational collapse of the plasma gas is thought to be responsible for the formation of giant molecular clouds in the Galaxy. The process of clump formation in the ISM near the Galactic plane is investigated. The initial ISM is assumed to consist of two fluids: plasma gas and cosmic-ray particles, in hydrostatic equilibrium, coupled with a uniform, azimuthally-aligned magnetic field. The evolution of the instability is explored in two models: an isothermal exponential-declining density model and a two-layered, hyperbolic tangent temperature model. After a small perturbation, the unstable gas aggregates at the bottom of the magnetic loops and forms dense blobs. The growth rate of the instability decreases as the coupling between the cosmic rays and the plasma becomes stronger (meaning a smaller CR diffusion coefficient). The mixing is enhanced by the cosmic-ray diffusion, while the shape of the condensed gas depends sensitively on the initial equilibrium conditions. In the hyperbolic tangent temperature model, a more concentrated and round shape of clumps like the giant molecular cloud is observed at the foot points of rising magnetic arches. Conversely, in the exponential density model, a filamentary morphology of the clumpy structure is attained.

Keywords: cosmic rays, magnetohydrodynamics (MHD), instability, numerical simulation

1. Introduction

Parker (1966) first identified the instability of a gravitationally stratified gaseous disk in a magneto-hydrostatic equilibrium, like the Galaxy, in response to perturbations due to magnetic buoyancy, if perturbations occur in the magnetic field lines that lie parallel to the disk plane. This phenomenon is referred to as magnetic buoyancy instability (Hughes & Proctor 1988; Tajima & Shibata 1997) or, in astronomical literature, Parker instability (Parker 1966; 1979). Solar magnetic activities such as sunspots, which is attributed to the emergence of magnetic flux tubes from the interior of the sun into the solar atmosphere (Zwaan 1985, 1987), also reflect this instability. Early observational evidence related to Parker instability had been proposed by Appenzeller (1971). Giant dense CO molecular loops close to the Galactic center support Parker instability (Fukui et al., 2006). As is expected, gas aggregating at the foot-point of the rising magnetic loops eventually collapses, becoming a giant cloud and a region that hosts stellar formations. A more recent findings of the mushroom shape of the hydrogen cloud GW 123.4-1.5 Baek, Kudoh & Tomisaka (2008) also suggested magnetic floatation and, hence, Parker instability. However, Hanasz et al. (2004) found that for galactic dynamo models, the efficiency of sustaining the galactic magnetic field can be improved if the effect of cosmic rays is incorporated. Actually, in Parker's original concept of instability, the role of cosmic rays has been considered, because the cosmic-ray pressure functions just like the magnetic pressure, capable of overpowering the gas pressure inside the magnetic flux tube and making it easier for the gas to rise.

Cosmic rays are a major component in the interstellar medium (ISM) in galaxies, whose energy density is comparable to the kinetic and magnetic energy densities of thermal plasma gas (Ferriére 2001). Cosmic rays are high energy particles, of which, 90% are protons. As long as their gyroradius is significantly smaller than the characteristic spatial scales of the magnetic field, cosmic rays particles only propagate along the magnetic

Email address: yueh@phys.cycu.edu.tw; cw5b@msn.com (Chih-Yueh Wang)

field lines. Although the velocity of cosmic-ray particles is close to the speed of light, the bulk motion of cosmic rays is diffusive and the bulk speed is of the order of Alfvén speed.

The morphology of this instability can exhibit two modes, i.e. the undular mode (the wavenumber vector $k\|$ of the perturbation parallel to the magnetic field B), and the interchange mode ($k\perp$ perpendicular to B). The undular mode, also called Parker instability, is excited by perturbations along the magnetic field lines, where the falling gas creates a magnetic buoyancy greater than the restoring magnetic tension. However, the interchange mode, known as flute instability or magnetic Rayleigh-Taylor instability (Kruskal & Schwarzchild 1954), occurs for shorter-wavelength perturbations, capable of causing two straight flux tubes to interchange and ultimately reducing the potential energy in the system. The linear growth rate of the interchange mode generally exceeds that of the undular mode owing to the short wavelength. However, in the nonlinear stage, the undular mode often dominates (Matsumoto et al, 1993; Tajima & Shibata 1997). Thus, the undular mode (Parker instability) is more important than the interchange mode in astrophysical problems.

Baierlein (1983) and Matsumoto et al. (1988) performed the first one- and two-dimensional (2D), pure MHD simulations of Parker instability, respectively. The findings are that in the nonlinear stage, the gas condensates to form giant clouds; in addition, a shock wave appears in the flow along the rising magnetic loop. By applying the simulation results of Matsumoto et al. (1988) to the solar atmosphere, Shibata et al. (1989b, 1990a) demonstrated that the emerging magnetic loop still expands self-similarly during the nonlinar evolution in two dimensions. Kamaya et al. (1996) adopted the supernova explosion as a perturbation in the ISM to trigger nonlinear instability. Earlier, Nozawa (1992) also examined the instability deeper in the convectively unstable layer of the solar atmosphere; when considering how magnetic shear affects the flow (Hanawa, Matsumoto, & Shibata 1992; Nozawa 2005), although the interchange mode is stabilized, a large thin-structure may still form. Shantanu et al. (1997) and Kim et al. (2000) made a further application of Parker instability to the Galactic disk without cosmic rays.

In Parker's original analysis, the instability has a maximum growth rate for non-zero $k\perp$, although non-zero $k\|$ is the main cause for the instability. In the 3D simulations for both solar and galactic problems by Matsumoto & Shibata (1992) and Matsumoto et al. (1993), the previous 2D results of cloud formation, presence of shock wave, and self-similar evolution are confirmed. However, the spatial and temporal scale in these studies depends on the $k\perp$. If a larger $k\perp$ is applied, the magnetic loop tends to have a thinner structure and a horizontal expansion, which would suppresses the upward expansion (Matsumoto et al. 1993). Similarly thin structures have been found in other 3D simulations of Kim et al. (1998, 2001, 2001) and Hanasz et al. (2002).

This study describes the evolution of Parker instability undergoing cosmic-ray diffusion using 2D simulations. Effects of the adiabatic index and the initial hydrostatic condition other than an isothermal temperature and a uniform density profile are examined. Two initial profiles are used, i.e. the hyperbolic tangent temperature model, i.e. often used in the solar atmosphere, and the exponential density model, i.e. appropriate for Galactic problems. Various perturbation results are also explored. The physical parameters and initial conditions invoked are particularly appropriate for a galactic ISM. Section 2-5 details the governing equations, initial conditions, and numerical approaches. Section 6 describes the numerical algorithms results, while Section 7 discusses the results. Conclusions are finally drawn.

2. Governing Equations

This study investigates how cosmic rays affect a MHD system. In this hydrodynamic approach, the cosmic rays and the thermal plasma are two fluid components of a plasma system; the plasma fluid has a mass density of ρ, a thermal pressure of P_g and a cosmic-ray pressure of P_c, all of which are threaded by a frozen-in magnetic field $\mathbf{B}$. The cosmic-ray energy is described based on the diffusion-convection equation (Drury & Völk 1981; Jones & Kang 1990), with the cosmic rays treated as a hot massless fluid. Additionally, the momentum spectrum of cosmic rays is neglected to simplify the governing equations. The artificial separation of the cosmic rays from the plasma helps to distinguish the role played by high- and low-energy components.

This study investigates the Parker instability with respect to how cosmic rays affect a uniformly-rotating disk, with each fluid element under the influence of external gravity from the Galactic center. Self-gravity from the plasma gas is not included. A local rectangular domain representing the corotating sheet of the Galactic disk in the vertical plane is used for the simulations. The horizontal component of the radially inward external gravity is balanced by the centrifugal force. Therefore, in the momentum equation, only the vertical component of external gravity and the Coriolis force are present to account for the rotation.

The cosmic-ray diffusion-convection equation supplements the standard set of ideal MHD equations. The governing equations are written as

$$\frac{\partial \rho}{\partial t} + \nabla \cdot (\rho \mathbf{V}) = 0, \quad (1)$$

$$\frac{\partial \rho \mathbf{V}}{\partial t} + \nabla \cdot \left[\rho \mathbf{V}\mathbf{V} + (P_g + P_c + \frac{B^2}{8\pi})\mathbf{I} + \frac{\mathbf{B}\mathbf{B}}{4\pi} \right] - \rho \mathbf{g} + 2\rho \mathbf{\Omega} \times \mathbf{V} = 0, \quad (2)$$

$$\frac{\partial \mathbf{B}}{\partial t} + \nabla \times (\mathbf{V} \times \mathbf{B}) = 0, \quad (3)$$

$$\frac{\partial}{\partial t}(\frac{P_g}{\gamma_g - 1} + \frac{1}{2}\rho V^2 + \frac{B^2}{8\pi}) + \nabla \cdot \left[(\frac{\gamma_\mathbf{g}}{\gamma_\mathbf{g} - \mathbf{1}}\mathbf{P_g} + \frac{\mathbf{1}}{\mathbf{2}}\rho V^2)\mathbf{V} + \frac{c}{4\pi}\mathbf{E} \times \mathbf{B} \right] + \mathbf{V} \cdot (\nabla P_c - \rho \mathbf{g}) = 0, \quad (4)$$

$$\frac{\partial}{\partial t}(\frac{P_c}{\gamma_c - 1}) + \nabla \cdot (\frac{\gamma_c}{\gamma_c - 1} P_c)\mathbf{V} - \mathbf{V} \cdot \nabla P_c - \nabla \cdot \left[\overleftrightarrow{\kappa} \nabla (\frac{P_c}{\gamma_c - 1}) \right] = 0. \quad (5)$$

where $\mathbf{V}$ denotes the plasma fluid velocity; $\mathbf{I}$ denotes a unit tensor; γ_g denotes the adiabatic index, i.e. ratio of the heat capacity at a constant pressure to that at a constant volume, of the thermal plasma gas; γ_c refers to the adiabatic index of the cosmic rays; $\overleftrightarrow{\kappa}$ represents the cosmic-ray diffusivity; $\mathbf{\Omega}$ represents the rotation angular frequency; and $\mathbf{g}$ is the external gravitational acceleration. Deriving this equation set involves use of the distribution function in Vlasov equation skilling75; it has also been used in Kuwabara, Nakamura & Ko (2004), and Lo, Ko & Wang (2010).

Notably, in addition to balancing the energy equations, the term cosmic-ray pressure P_c affects the momentum equation Eq.(2). However, particles of cosmic rays do not interaction with plasma directly; they interact with plasma via the magnetic field. On a microscopic scale, resonant scattering of Alfvén waves keeps the cosmic rays nearly isotropically distributed everywhere with respect to the thermal plasma background. A situation in which the cosmic-ray pressure possesses a gradient ∇P_c influences the motion of the plasma gas. Thus, the interaction of cosmic-ray particles with a thermal plasma can be represented by the cosmic-ray pressure P_c and its gradient. The transport of the cosmic-ray pressure is described by a macroscopic diffusion coefficient, $\overleftrightarrow{\kappa}$, an energy-weighted mean diffusion tensor, defined as

$$\overleftrightarrow{\kappa} = (\kappa_\parallel - \kappa_\perp)\hat{b}\hat{b} + \kappa_\perp \delta_{ij}, \quad (6)$$

where $\hat{b}$ denotes a unit vector along the $\mathbf{B}$ direction.

This model is limited mainly in that one must assume a priori knowledge of the cosmic-ray pressure and energy density that satisfies the adiabaitc index $\gamma_c = 1 + P_c/E_c$. Here, Eqs.(1)-(5) are solved numerically in a local reference frame in Cartesian coordinates, whose center lies at a galactocentric radius R_o and orbits the galaxy with a fixed angular velocity $\Omega = \Omega(R_o)$. In this local frame, the radial, azimuthal, and vertical spatial coordinates are related to the Cartesian coordinates such that $x = R - R_o$, $y = R_o(\phi - \Omega\, t)$, and z=z.

3. Normalization

The parameters and variables used in the governing equations withstand an extremely large contrast when expressed in dimensional units, possibly incurring significant errors and thus infeasible for numerical calculations. To overcome such numerical difficulties, the above equations are normalized to non-dimensional values that are close to unity. The non-dimensional values is denoted by the superscript "$*$" while the scaling factors are denoted by a "0" subscript. Some of the scaling factors also represent the quantities in equilibrium at the midplane of the Galactic disk.

The length variables are scaled based on the pressure scale height H_0:

$$x^* = x/H_0\ ,\ y^* = y/H_0 \text{ and } z^* = z/H_0.$$

H_0 is determined by integrating the hydrostatic equilibrium equation:

$$-\int_{P_{g0}}^{P_{g0/e}} \frac{dP_g}{P_g} = \int_0^{H_0} \frac{\gamma_g\ g_z}{C_{s0}^2(1 + 1/\alpha + 1/\beta)} dz,$$

given the values of sound speed C_{s0}, the gravitational acceleration g_z in the z-direction, the ratio of plasma pressure to magnetic pressure α, the ratio of plasma pressure to cosmic-ray pressure β; and γ_g. The gas at the Galactic disk plane is nearly isothermal such that $\gamma_g \approx 1.0$. The sound speed at the disk plane is

$$C_{s0} = 10 \text{ (km/s)} = 1.0 \times 10^6 \text{ (cms}^{-1}\text{)}. \quad (7)$$

Thus, for $\alpha = \beta = 1$ and $g_z = 2.28 \times 10^{-8}$ (cms^{-2}),

$$H_0 = 50 \text{ (pc)} = 1.54 \times 10^{20} \text{ (cm)}. \quad (8)$$

Given C_{s0}, the velocity is normalized to $V^* = V/C_{s0}$, and the time scaling factor τ_0 is defined as H_0/C_{s0}.

$$\tau_0 = H_0/C_{s0} = 1.54 \times 10^{14} \text{ (sec)} \sim 5 \text{ (Myr)}. \quad (9)$$

The ISM density is used to normalize the density, with ρ_0 being about one atom per cubic cm in the ISM, or

$$\rho_0 = 1.6 \times 10^{-24} \ (\mathrm{gcm}^{-3}), \tag{10}$$

Given the above scalings, the mass equation Eq.(1) is rewritten as

$$\partial(\rho_0\rho^*)/\partial(\tau_0 t^*) + 1/H_0 \nabla^* \cdot (\rho_0 \rho^* C_{s0} \mathbf{V}^*) = \mathbf{0},$$

which is then converted into $\partial\, \rho^*/\partial\, t^* + \nabla^* \cdot (\rho^* \mathbf{V}^*) = \mathbf{0}$ using Eq.(9).

Similarly, the factor $\rho_0 C_{s0}/(H_0/C_{s0}) = \rho_0 C_{s0}^2/H_0$ at the left hand side of the momentum equation Eq.(2) is balanced by the same factor at the right hand side. The normalized plasma gas pressure is $P_g^* = P_g/P_{g0}$, where

$$P_{g0} = C_{s0}^2 \rho_0 = 1.6 \times 10^{-12} \ (\mathrm{g\ cm^{-2}\ s^{-2}}), \tag{11}$$

and so the gradient of plasma pressure becomes $\frac{\rho_0 C_{s0}^2}{H_0} \nabla^* P_g^*$.

Scaling of the cosmic-ray pressure also employs the gas pressure, $P_c^* = P_c/P_{g0}$. The scaling factor for the magnetic field, B_0, is determined by $B_0^2 = P_{g0}$, and for the Galaxy,

$$B_0 = \sqrt{P_{g0}} = 1.26 \times 10^{-6} \ (\mathrm{gauss}). \tag{12}$$

In order normalize the momentum equation, the gravitational acceleration is scaled to

$$g_0 = \frac{C_{s0}^2}{H_0} = 6.49 \times 10^{-9} \ (\mathrm{cms}^{-2}), \tag{13}$$

while the scaling factor for the rotating angular frequency is the reverse of time:

$$\Omega_0 = \frac{C_{s0}}{H_0} = 0.65 \times 10^{-26} \ (\mathrm{s}^{-1}). \tag{14}$$

Using Eq.(8) to (14), the momentum equation Eq.(2), the induction equation Eq.(3) and energy equation Eq.(4) can all be converted to dimensionless values.

Finally, in Eq.(5), the cosmic-ray diffusion coefficient κ is normalized to $\kappa^* = \kappa/\kappa_0$, where

$$\kappa_0 = C_{s0} H_0 = 1.54 \times 10^{24} \ (\mathrm{cm^2 s^{-1}}), \tag{15}$$

and a maximum value of $\kappa^* = 200$ is used.

4. Initial Equilibrium Backgound

This study adopts two initial equilibrium backgrounds: a temperature distribution that follows a hyperbolic tangent profile and a density distribution that follows an exponential profile. Both of these backgrounds bear a declining density profile with height. These backgrounds differ mainly in that the hyperbolic tangent model has a transition zone that divides the distribution into two distinct regions, while the exponential model shows a smooth distribution. Given the temperature or density profile, the profiles for the density/temperature, pressure, magnetic field and other variables are derived from the hydrostatic equation.

In the isothermal case the criteria for Parker instability to grow is $\frac{d}{dz}(B/\rho) < 0$. When the rising field lines grow, the flow becomes unstable. In our cases, the growth of the instability depends on additional parameters such as the width of transition region and the height of Galactic halo (disk thickness).

4.1. Hyperbolic Tangent Temperature

The hyperbolic tangent temperature profile is a two-temperature, layered disk (Shibata et al. 1989a), described by

$$C_s^2(z) = T(z) = T_0 + (T_h - T_0)\frac{1}{2}[\tanh(\frac{z - z_h}{w_{tr}}) + 1],$$

where $C_s(z)$ is the sound speed, $T_0 = 10^4$ (K) is the disk temperature and $T_h = 25T_0$ is the halo temperature. The initial dimensionless temeprature is 1.0, equivalent to 10^4 (K). Given the ideal gas law $P_g = \frac{\rho T}{\gamma_g}$ and the gravitational acceleration g_z, the initial density profile is solved using the hydrostatic equation

$$\frac{d}{dz}[(1 + \frac{1}{\alpha} + \frac{1}{\beta})P_g] + \rho g_z = 0. \tag{16}$$

A constant acceleration g_z is assumed because the grid domain is small and not far way from the disk plane. The dimensionless gravitational acceleration is set as $1.0/\gamma_g$ (dimensionless units), equivalent to $6.49/\gamma_g \times 10^{-9}$ (cms^{-2}), or $\sim 6.18 \times 10^{-9}$ (cms^{-2}), if $\gamma_g = 1.05$. Notably, this value is a little higher than the value derived from observations of the spatial density distribution and the velocity-distance correlation 500 pc above the disk midplane, 4×10^{-9} cms^{-2} (Oort 1960; Bahcall 1984; Kuijken & Gilmore 1989). Nevertheless, gravitational acceleration can vary widely from galaxy to galaxy. The initial density at the disk plane is 1.0 (dimensionless units), equivalent to $1.6 \times 10^{-24} (g/cm^3)$.

After obtaining the density profile, the plasma pressure profile $P_g = C_s^2 \rho/\gamma_g$ is dervied. The magnetic feld is assumed to align in the x-direction and vary with height z, and $B_x(z) = \sqrt{8\pi P_g/\alpha}$.

The initial dimensionless pressure at the disk is 1.0, (2×10^{-12} ($\mathrm{g\ cm^{-2}\ s^{-2}}$)). The initial magnetic field at the disk for $\alpha = 1$ is $\sqrt{8\pi} \sim 5$ (dimensionless units), or $5B_0 = 6.34$ (μ gauss), This field strength is very close to

the radio synchrotron measurement of 6 (μ gauss) averaged over a radius of about 1 kpc around the Sun (Beck 2009) .

The initial cosmic-ray pressure at disk for $\beta = 1$ is 1.0 (dimensionless units), or 2×10^{-12} (g cm^{-2} s^{-2}). The rotating angular frequency Ω (not used in this work) is a free parameter; $\Omega^* = 1$ gives 0.65×10^{-26} (s^{-1}), or approximately 7 times the angular freguency at our Sun, $\Omega_\odot = 220/7.6$ (km s^{-1}/kpc).

5. Grid Setup and Perturbation

2D simulations are performed in a rectangular domain in the $x-z$ plane. To excite the instability, velocity perturbations are added to the quiescient background. Two perturbation forms are examined: eigen mode sinusoidal wave and random seed.

The sinusoidal perturbation employs a perturbing velocity V_x described by

$$V_x = 0.05\ C_{s0}\ \sin(\frac{2\pi(x-x_0)}{\lambda}), \tag{17}$$

where $\lambda = 20H_0$ is the most unstable wavelength derived from the linear analysis for $\kappa_\parallel = 200$ (Kuwabara, Nakamura & Ko 2004). V_x is applied within the region of $4H_0 < z < 8H_0$ and $|x - x_0| < 1/2\lambda$, where $x_0 = 40$ (dimesionless unit). The grid consists of $102 \times\ 301$ zones in a rectangular region of 4 (kpc)$\times$3.5 (kpc). The horizontal length of each grid zone is $\Delta x = 0.8H_0$, while the vertical length is nonuniform:

$$\Delta z = \begin{cases} 0.15H_0, & 0 \le z < 25H_0 \\ min\{1.05\Delta z, \Delta z_{max}\}, & \text{otherwise} \end{cases},$$

Δz is increased above $z = 25H_0$ by a ratio of 1.05, until $\Delta z_{max} = 5\Delta\ z$ ($at\ z = 0$). The upper grid domain accomodates the unperturbed magnetic field, and so spurious outflows across the grid boundary is avoided.

For the random velocity perturbation (Shore & Larosa 1999), a series of random velocities V_x and V_z with a maximum amplitude of 5% is added horizontally into the background (Chou et al. 2000). The grid covers an area of 9 (kpc) $\times$ 11.5 (kpc) using $512 \times\ 512$ zones, with $\Delta x = 0.35H_0$ and

$$\Delta z = \begin{cases} 0.15H_0, & 0 \le z < 35H_0 \\ min\{1.05\Delta z, \Delta z_{max}\}, & \text{otherwise} \end{cases}.$$

6. Numerical Algorithms

A hybrid finite difference method called *time Splitting method* or *operator splitting method* is employed to solve the equations. Eqs.(1-4), are in the flux-conservative form and are solved by 2-Steps Lax-Wendroff explict method. The cosmic-ray energy equation Eq.(5) is divided into the convection and diffusion parts. The convection part is first converted to a conservative form and then also solved by 2-Steps Lax-Wendroff explict method. The diffusion part is sovled by the biconjugate gradients stabilized (BICGStab) implicity method.

In the 2-step Lax-Wendroff method, Eqs.(1-4) and the convection part of Eq.(5) are rewritten in the conservative form:

$$\frac{\partial U}{\partial t} + \frac{\partial F}{\partial x} + \frac{\partial G}{\partial y} + \frac{\partial H}{\partial z} = S, \tag{18}$$

where U can be density ρ, momentums $\rho\mathbf{V}$, energy E_g and magnetic field $\mathbf{B}$; F,G,H are the flux of U in x-,y-,z-direction; and S is the source term. The x component of Eq.(18) is split into two steps:

$$\begin{cases} \frac{U^{n+1/2}_{i+1/2} - \frac{U^n_i + U^n_{i+1}}{2}}{1/2\Delta t} + \frac{F^n_{i+1} - F^n_i}{\Delta x} + S^n_i = 0 \Big\} Step1 \\ \frac{U^{n+1}_i - U^n_i}{\Delta t} + \frac{F^{n+1/2}_{i+1/2} - F^{n+1/2}_{i-1/2}}{\Delta x} + S^{n+1/2}_i = 0 \Big\} Step2. \end{cases} \tag{19}$$

where superscript n denotes time advection and subscript i represents space grid.

The diffusion part of Eq.(5) is written as:

$$\frac{\partial E_c}{\partial t} - \nabla \cdot \left[\overleftrightarrow{\kappa}\nabla(E_c)\right] = 0,$$

whose finite-difference form is expressed as $\mathbf{Ax} = \mathbf{b}$, where the submatrix in $\mathbf{A} = [\mathbf{A}_1, \mathbf{A}_2, \mathbf{A}_3, \mathbf{A}_4, \mathbf{A}_5, \mathbf{A}_6, \mathbf{A}_7]$ and the vector $\mathbf{b}$ is the function of time step Δt, the cosmic-ray diffusion coefficient $\overleftrightarrow{\kappa}$, the magnetic field $\mathbf{B}$ and the cosmic-ray energy E^n_c at the nth iteration. The vector $\mathbf{x}$ is the unknown:

$$\begin{aligned} \mathbf{x} = \ & [E^{n+1}_{c,i,j,k-1}, E^{n+1}_{c,i,j-1,k}, E^{n+1}_{c,i-1,j,k}, E^{n+1}_{c,i,j,k}, \\ & E^{n+1}_{c,i+1,j,k}, E^{n+1}_{c,i,j+1,k}, E^{n+1}_{c,i,j,k+1}]^T. \end{aligned} \tag{20}$$

In order to solve $\mathbf{x}$ in Eq.(20), the BICGStab (Bi-Conjugate Gradient Stabilized) method is employed. This method can handle asymmetric linear systems and reduce the operations per iteration to $O(N^2)$, where N is the number of unknowns in the discretized domain, and is more efficient than the direct solution methods such as LU decomposition, which require $O(N^3)$ operations. The BICGStab is an iteration method that uses an initial guess $\mathbf{x}^0$ to find a corresponding residual $\mathbf{r}^0 = \mathbf{b} - \mathbf{Ax}^0$, and then iterate to the i-th step $\mathbf{r}^i$ to an accepted value by means of bi-conjugate matrix-vector

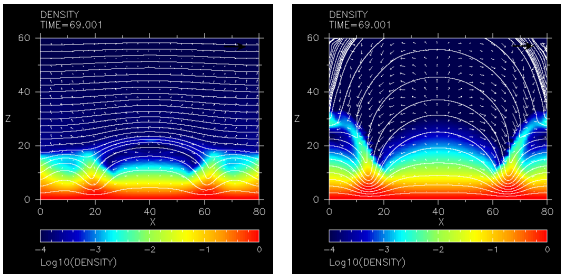

(a) (b)

Figure 1: Density contours at $t \sim 69$ for (1) a case of hyperbolic tangent temperature; (b) a case of exponential density.

operation. For comparison, when solving the nonlinear system $F(y) = 0$ with Newton's method:

$$y_i = y_{i-1} - \frac{F(y_{i-1})}{F'(y_{i-1})} = y_{i-1} + \delta_i,$$

the correction δ_i is determined by solving the gradient of the function, whereas in the BICGStab method,

$$\bar{r} = r_0 + \frac{||r_0||}{||y_{i-1}||} y_{i-1},$$

is used for the iteration. The BICGStab treatment for cosmic-ray energy diffiusion equation is an implicit method, and thus the CFL condition is not affected.

7. Results

7.1. Sinusoidal Perturbation

This section examines how cosmic-ray diffusion affects Parker instability by comparing a series of pure MHD simulations with simulations that include the cosmic-ray effect. Figure 1 illustrates those results using sinusoidal eigen mode perturbations. Figure 1a presents the hyperbolic tangent temperature model, while Fig.1b displays the exponential density model at the same epoch. Also included in these figures is a grid domain of $z \leq 60$ that just lies within the maximum height of the magnetic loops. Logarithmic values of variables in a dimensionless unit are presented in color contours. White solid lines represent the magnetic field lines, and small white arrows refer to the velocity vectors. The superscript "*" denoting dimensionless values is omitted hereafter.

7.2. Cosmic-Ray Diffusion Coeffieicnt

Figure 2 compares the maximum height of the magnetic loops versus the cosmic-ray diffusion coefficient $\kappa_\parallel$ in both models at $t = 33$, when the numerical time step becomes very restrained. A maximum of $\kappa_\parallel = 200$ (1.54×10^{24}(cm^{2}s^{-1})) is examined. In both models, the instability becomes more prominent with an increasing $\kappa_\parallel$, and the mixing extends to a similarly maximum height of $z \sim 55$. Notably, since the gradient of cosmic-ray pressure ∇P_c declines with an increasing diffusivity, cosmic-ray diffusion facilitates flow instability. Kuwabara, Nakamura & Ko (2004) studied the instability in the hyperbolic tangent temperature case. Our simulations reach a similar outcome for the growth rate.

The perpendicular or cross field lines diffusion coefficient $\kappa_\perp$ (see Eq.6) is often substantially smaller than the parallel coefficient $\kappa_\parallel$, which is only around $2\% - 4\%$ of $\kappa_\parallel$. Notably, even at a value of 2% of $\kappa_\parallel$, the effect of $\kappa_\perp$ on the mixing is significant (Fig. 3a and 3b). However, this finding contradicts the estimate made by linear analysis (Ryu et al. 2003). The role of cosmic rays makes us speculate whether Parker instability contributes to the galactic wind flow perpendicular to the galactic disk.

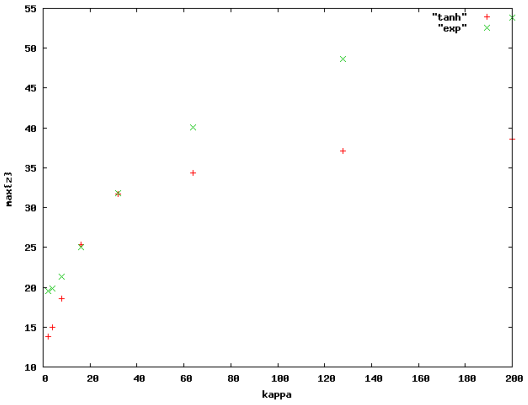

Figure 2: Maximum height of loops z versus cosmic-ray diffusion coefficient $\kappa_\parallel$.

7.3. Parameter α and β

The scale height H_0 in Eq.(8) is a set for $\alpha = \beta = 1$. Varying $\alpha = P_g/P_B$ modifies the length scale, resulting in different flow structures. Figure 4 presents snapshots of the hyperbolic tangent temperature model with $\alpha = 10.0$, which displays more prominent mixing than the $\alpha = 1$ case. Other parameters used are $\beta = 1.0$; $\gamma_g = 1.05$; $\gamma_c = 4/3$; $w_{tr} = 0.6$ (dimensionless units, 30 (pc) or 0.92×10^{20} (cm); $z_h = 18$ (900 (pc) or 1.39×10^{23} (cm)); $\kappa_\parallel = 2.0$ (1.54×10^{23} (cm^{2}s^{-1})); and $\kappa_\perp = 0.0$.

7.4. Parameter γ_g and w_{tr}

The temperature distribution is assumed to be uniform in the exponential density model. In this case,

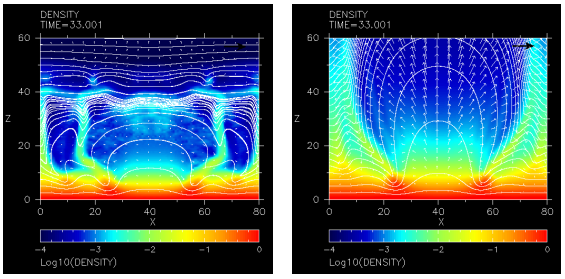

(a) (b)

Figure 3: Density contours at $t \sim 33$ for (a) hyperbolic tangent temperature model; (b) exponential density model.

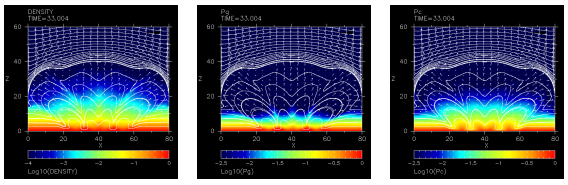

(a) $\log\rho$ (b) $\log P_g$ (c) $\log P_c$

Figure 4: Snapshots of density, pressure, and cosmic-ray pressure contours for hyperbolic tangent temperature model at $t \sim 33$ with $\alpha = 10$.

modifying α and β changes only the isothermal temperature value. Notably, the parameter $\beta = P_g/P_c$ should also influence the scale length (see Eq.(8). However, because cosmic rays largely diffuse along the magnetic field lines, varying β does not significantly affect the scale height.

In our simulations, the isothermal case is approximated using a minimum adiabatic index of $\gamma_g = 1.01$, where $\gamma_g = 1.0$. In an ISM, γ_g should be significantly smaller than the ideal value $5/3$ and close to 1.0, because thermal instability smoothens out the temperature gradient. However, because the diffusion of cosmic rays along the magnetic field lines is only slight and the instability growth expedites for more condensed gas, thermal instability is expected to be deterred when cosmic-ray diffusion is present (Shadmehri 2009). This finding may resemble the effect of increasing γ_g above the typical value 1.05 used in most of the simulations for Parker instability. According to our results, instability is dampened as γ increases; with $gamma = 5/3$, the flow remains quiescient at $t \times 98$ (Fig. 5a).

The criterion for Parker instability to occur is $\frac{d}{dz}(B/\rho) < 0$. In the hyperbolic tangent temperature model, an increasing width of transition region w_{tr} makes the instability less feasible (Fig. 5b). Suppression of the instability is attributed to the rapid rise of

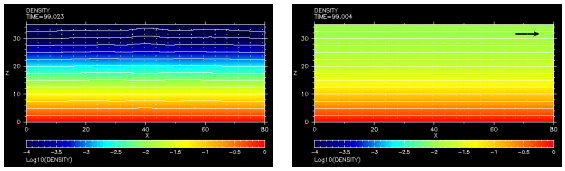

(a) $t \sim 98$, $\gamma_g = 5/3$ (b) $w_{tr} = 10.0$

Figure 5: Density contours for (a) $\gamma_g = 5/3$ and (b) $w_{tr} = 10.0$ in a hyperbolic tangent model.

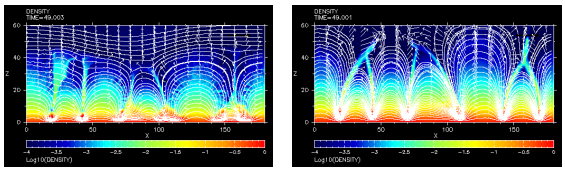

(a) (b)

Figure 6: Density contours at $t \sim 49$ for (a) hyperbolic tangent temperature (b) exponential density, (based on use of OR using) random perturbation.

temperature and the flattening of density near the transition region.

7.5. *Results of Random Perturbation*

The case using random velocity perturbation may reflect the circumstances closer to the actual situation in an ISM. Although in this case, the development of instability is less faster than the case using eigen mode perturbation, Fig. 6 reveals that strong mixing and filamentary structures are induced in both models.

7.6. *Trebly Sinusoidal Perturbation with $\kappa_\perp$*

When incorporating cosmic-ray cross field line diffusion $\kappa_\perp$, the magnetic field lines are aligned more vertically to the disk. As such a process may be related to the acceleration of galactic wind, a new initial condition using the same equilibrium background is invoked to examine the case involving $\kappa_\perp$.

A grid of 512×512 zones in a domain of 9(kpc) $\times$ 11.5(kpc) is adopted, with each zone having a size identical to the case of random perturbation. The applied velocity perturbation is similar to our previous sinusoidal eigen mode perturbation, but within a finite rectangular region of $|x - x_0| < 3/2\lambda$, where $x_0 = 90.0$, along with other similar parameters: $w_{tr} = 0.6$; $z_h = 18$; $\alpha = \beta = 1$; $\gamma_g = 1.05$; $\gamma_c = 4/3$; $\kappa_\parallel = 2.0$; and $\kappa_\perp = 0.0$.

Figure 7 shows the exponential case at the dimensionless time $t \sim 30$ (150 (Myr)). Three equally-sized loops arise and extend to $z \geq 50$. The flow pattern resembles

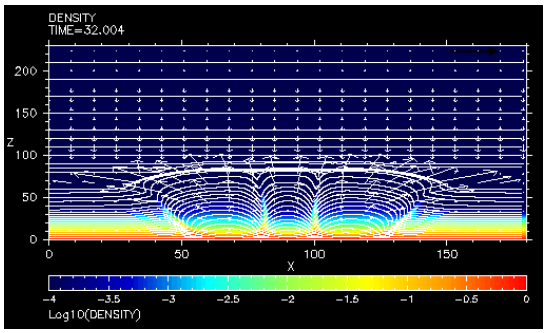

Figure 7: Density contour of the exponential density model at $t \sim 32$ using trebly sinusoidal perturbation and a cosmic-ray cross field line diffusion $\kappa_\perp$.

the hyperbolic tangent case in Kuwabara et al. (2004). At $t \sim 40$ the interaction between loops is more pronounced; the central one becomes compressed by two outer adjacent loops, while the loops continually rise to a height of 2.0 (kpc). At $t = 60$, the flow reaches a maximum vertical height and becomes saturated. Different from the case without $\kappa_\perp$, the velocity of the flow is very high, indicating that Parker instability is likely to contribute to the galactic wind acceleration (Wiegelmann, Schindler & Neukirch 1997).

8. Conclusion

This study has elucidated the development Parker instability undergoing cosmic-ray diffusion using 2D MHD simulations. Exactly how the initial conditions affect the growth of instability is also examined. Two equilibrium backgrounds are constructed based on hyperbolic tangent temperature and exponential density. Additionally, the instability is examined using variations in the physical parameters and perturbations.

Simulations are performed to reproduce the observed filaments near the Galactic center and the physical conditions giving rise to the structure, which closely resembles the long, thin wave-like sheared helmet plumes in the solar corona, caused by magnetic buoyancy (Shore & Larosa 1999). The perpendicular component of cosmic-ray diffusion coefficient $\kappa_\perp$ is included as well. When $\kappa_\perp$ is only $1\% - 2\%$ of the parallel component $\kappa_\parallel$, despite their development, vertical magnetic structures and outward flow arise, particularly in the exponential density model. The morphology of the clumpy structure is filamentary. Conversely, in the hyperbolic tangent temperature model, a more concentrated and round shape of clumps like the giant molecular cloud are observed at the foot points of rising magnetic arches. Notably, the growth of instability in the hyperbolic tangent model is less rapid than that of the exponential density case since the pressure in the exponential density decreases faster with an increasing height.

The small gradient of cosmic ray pressure along the z direction caused by diffusion explains why an increase in $\kappa_\parallel$ facilitates the growth of the unstable undular mode. Consequently, the gas falls down more rapidly, and adjacent loops join together to form a large loop-like bubble.

Exponential density with the adiabatic index $\gamma_g \sim 1$ (i.e. isothermal) produces the highest magnetic loops and most flow instability. A decreasing γ_g decreases leads to more condensed gas and, ultimately, a more unstable flow. While examining a situation without cosmic-ray diffusion, Parker indicated that the criterion for instability is $\gamma_g < 1.36$. Although the undular mode is expected to be suppressed when $\gamma_g > 1.4$, in our cases using $1.3 < \gamma_g < 1.4$, numerical results indicate that the high adiabatic index still produces a non-uniform density distribution. Such instability may still occur if a stronger perturbation such as a supernova explosion is invoked.

The hyperbolic tangent temperature model yields a density distribution that increases with height, whose steepness depends on the width of the transition zone w_{tr}. For a smaller w_{tr}, instability is increased as the density gradient correspondingly diminishes near the unstable regions.

Applying a larger ratio of plasma pressure to magnetic pressure α diminishes the pressure inside the flux tube, thus facilitating the growing instability. Also, the length scale decreases, and unstable structures are observed on a smaller scale. In contrast, a small α yields a larger scale height, complicating the mixing of an unstable flow.

Finally, in the proposed model, the ratio of plasma pressure to cosmic-ray pressure β does not influence the length scale since the diffusion of the cosmic-ray pressure does not contribute to the scale height.

Acknowledgment

We thank the National Science Council of Taiwan for funding this project, and the National Center for High-Performance Computing Center for providing computing facilities.

References

[1] I. Appenzeller,*Observational Evidence for Parker's Instability of the Interstellar Gas and Maguetic Field* Astron. Astrophys., 12, (1971), pp. 313-315

[2] C. H. Baek, T. Kudoh & K. Tomisaka, *How was the mushroom-shaped GW* 123.4 – 1.5 *formed in the Galactic disk?* Astrophys. J., 682, (2008), pp. 434-444

[3] R. Baierlein, MNRAS, 205 (1983) 669

[4] J. N. Bahcall, *Self-consistent determinations of the total amount of matter near the sun* Astrophys. J., 276, (1984), pp. 169-181

[5] R. Beck, *Galactic and extragalactic magnetic fields – a concise review* Astrophys. Space Sci. Trans., 5 (2009), pp. 43-47

[6] W. Chou, R. Matsumoto, T. Tajima, M. Umekawa & K. Shibata, *Dynamics Of The Parker-Jeans Instibility In A Galactic Gaseous Disk* Astrophys. J., 538 (2000), pp. 710-727

[7] L'OC Drury & H. J. Völk, *Hydromagnetic shock structure in the presence of cosmic rays* Astrophys. J., 248, (1981), pp. 344-351

[8] K. M. Ferriére, *The interstellar environment of our galaxy* Rev. Mod. Phys., 3, (2001), pp. 1031-1066

[9] Y. Fukui, et al. *Molecular Loops in the Galactic Center: Evidence for Magnetic Flotation* Science, 314, (2006), pp. 106-109

[10] M. Hanasz, K. Otmianowska-mazur, H. Lesch, A&A, 386 (2002), 347

[11] M. Hanasz, G. Kowal, K. Otmianowska-Mazur and H. Lesch, *Amplification of Galactic Magnetic Fields by the Cosmic-Ray-driven Dynamo* Astrophys. J., 605 (2004), pp. L33-L36

[12] T. Hanawa, R. Matsumoto, & K. Shibata. ApJ, 393 (1992), L71

[13] D. W. Hughes, & M. R. E. Proctor, Annual Review of Fluid Mechanics, 20, (1988), 187

[14] T. W. Jones, & H. Kang, *Time-dependent evolution of cosmic-ray-mediated shocks in the two-fluid model* Astrophys. J., 363, (1990), pp. 499-514

[15] H. Kamaya, S. Mineshige, K. Shibata, & R. Matsumoto, ApJ, 458 (1996), L25

[16] J. Kim, J. Franco, S. S. Hong, A. Santillan, & M. A. Martos, ApJ, 531 (2000), 873

[17] J. Kim, S. S. Hong, D. Ryu & T. W. Jones, *Three-dimension Evolution of The Parker Instability Under A Uniform Gravity* Astrophys. J., 506 (1998), pp. L139-L142

[18] J. Kim, D. Ryu, & T. W. Jones, ApJ, 557 (2001), 464

[19] W. Kim, E. C. Ostriker, & J. M. Stone, ApJ, 581 (2002), 1080

[20] K. D. Kruskal, & M. Schwarzchild, Proc. R. Soc. London, Ser A., 223 (1954), 348

[21] K. Kuijken & G. Gilmore, *The Mass Distribution in the Galactic Disc - Part III - the Local Volume Mass Density* Monthly Notices Royal Astron. Soc., 239, (1989), pp. 651-664

[22] T. Kuwabara, K. Nakamura & C. M. Ko, *Nonlinear Parker Instability with The Effect of Cosmic-ray Diffusion* Astrophys. J., 607 (2004), pp. 828-839

[23] T. Kuwabara, K. Nakamura & C. M. Ko, Astrophysical Journal, 607, (2004), 828-839

[24] S. E. Lee, *Parker Instability in a Self-gravitating Magnetized Gas Disk: II. Competition between Gravitational and Convective Instabilities* New Astron., 14 (2009) pp. 44-50

[25] Y.-Y. LO, C.-M. Ko & C.-Y. Wang, *3-D Magneto-Hydrodynamic Simulations of Parker Instability with Cosmic Rays* Computer Physics Communications, Special Issue of CCP 2009, (2010), accepted.

[26] G. I. Marchuk, *Method of Numerical Mathematics vol. 2*, Springer-Verlag, Berlin (1975)

[27] R. Matsumoto, T. Horiuchi, K. Shibata, & T. Hanawa, PASJ, 40 (1988), 171.

[28] R. Matsumoto, & K. Shibata, PASJ, 44 (1992), 167

[29] R. Matsumoto, T. Tajima, W. Chou, K., A. Okubo, & K. Shibata, ApJ, 493 (1998), 414

[30] R. Matsumoto, T. Tajima, K., Shibata, & M. Kaisig, ApJ, 414 (1993), 357

[31] S. Nozawa, K. Shibata, R. Matsumoto, A.C. Sterling, T. Tajima, Y. Uchida, A. Ferrari, & R. Rosner, ApJS, 78, (1992), pp.267

[32] S. Nozawa, *Three-Dimensional Magnetohydrodynamic Simulation of Nonlinear Magnetic Buoyance Instability of Flux Sheets with Magnetic Shear*, Publ. Astron. Soc. Japan, 57, (2005), pp. 995-1007

[33] J. H. Oort, *Note on the determination of κ_z and on the mass density near the Sun* Bull. Astr. Inst. Netherlands, 15, (1960), pp. 45-53

[34] K. Otmianowska-Mazur, M. Soida, B. Kulesza-Żydzik, M. Hanasz & G. Kowal, *Can The Cosmic-ray Driven Dynamo Model Explain The Observations of The Polarized Emission of Edge-on Galaxies* Astrophys. J., 693 (2009), pp. 1-7

[35] E. N. Parker, *The Dynamical Stste of The Installermedium Gas and Field* Astrophys. J., 145 (1966), pp. 881-833

[36] E. N. Parker, Cosmical Magnetic Fields (1979), Oxford: Clarendon Press

[37] D. Ryu, J. Kim, S. S. Hong & T. W. Jones, *The Effect of Cosmic-rays Diffusion On The Parker Instability* Astrophys. J., 589 (2003), 338??46

[38] K. Shibata, T. Tajima, R. Matsumoto, T. Horiuchi, T. Hanawa, R. Rosner, and Y. Uchida, *Nonlinear Parker Instability of Isolated Magnetic Flux in a Plasma* Astrophys. J., 338 (1989), pp. 471-492

[39] B. Shantanu, T. Ch. Mouschovias, & E. V. Paleologou, ApJ, 480 (1997), 55 *Dynamical Effects of the Parker Instability in the Interstellar Medium*,

[40] K. Shibata, T. Tajima, R. S. Steinolfson, & R. Matsumoto, ApJ, 345 (1989), 584

[41] K. Shibata, S. Nozawa, R. Matsumoto, A. C. Sterling, & T. Tajima, ApJ, 351 (1990), L25

[42] K. Shibata, T. Tajima, R. Matsumoto, ApJ, 350 (1990), 295

[43] K. Shibata, & R. matsumoto, Nature, 353 (1991), 633

[44] S. N. Shore & T. N. Larosa, *The Galactic Center Isolated Nonthermal Filaments as Analogs of Cometary Plasma Tails* Astrophys. J., 521 (1999), 587-590

[45] M. Shadmehri, *Thermal instability and the effects of cosmic-ray diffusion* Monthly Notices Royal Astron. Soc., 397, (2009), pp. 1521-1527

[46] J. Skilling,*Cosmic ray streaming. III - Self-consistent solutions* Monthly Notices Royal Astron. Soc., 173, (1975), pp. 255-269

[47] T. Tajima, & K. Shibata, Plasma Astrophysics (1997), Reading, Massachusetts: Addison-Wesley

[48] T. Wiegelmann, K. Schindler & T. Neukirch, *Helmet Streamers with Triple Structures: Weakly Two-Dimensional Stationary States* Solar Phys., 180, (1997), pp. 439-460

[49] C. Zwaan, Sol. Phys., 100 (1985), 397

[50] C. Zwaan, Annual Review of Astronomy and Astrophysics, 25 (1987), 83